

Time-resolved measurements of the shock-compression response of Mo+2Si elemental powder mixtures

Kevin S. Vandersall

Lawrence Livermore National Laboratory, 7000 East Avenue L-282, Livermore, California 94550

Naresh N. Thadhani^{a)}

School of Materials Science and Engineering, Georgia Institute of Technology, 771 Ferst Drive, Atlanta, Georgia 30332-0245

(Received 10 January 2003; accepted 6 May 2003)

The shock-compression response of Mo+2Si elemental powder mixtures was investigated using instrumented experiments in the velocity range of 500 m/s to 1 km/s. The experiments employed polyvinyl difluoride stress gauges placed at the front and rear surfaces of the powder mixtures to determine the crush strength, densification history, and shock-induced reaction initiation characteristics. Experiments performed on $\sim 58\%$ dense Mo+2Si powder mixtures at input stresses less than 4 GPa showed characteristics of powder densification and dispersed propagated wave stress profiles with rise time $> \sim 40$ ns. At input stress between 4 and 6 GPa, the powder mixtures showed a shock-compression response following the Hugoniot of the solid-density mixture. In the stress regime of 6–7 GPa, shock-induced melting of silicon was observed, which appears to inhibit a shock-induced chemical reaction on the time scale of the time-resolved measurements. The results of the present work on Mo-Si, taken in conjunction with prior work on the Nb-Si and Ti-Si systems, illustrate that premature melting of silicon and its capillary flow can limit the deformation and mixing between reactants, thereby inhibiting the initiation of “shock-induced” chemical reactions. © 2003 American Institute of Physics. [DOI: 10.1063/1.1586968]

I. INTRODUCTION

Shock compression of powder mixtures can introduce physical, chemical, and physiochemical changes in microsecond-duration time scales of the peak-pressure state.¹ These so-called “shock-induced” changes, resulting in the formation of nonequilibrium compounds, metastable phases, or simply radically modified microstructures,^{2–5} have also received increasing interest in the area of energetic materials for the purposes of controlling the energy release rate.⁶ Shock initiation of chemical reactions in highly reactive powder mixtures has been proposed to occur as a consequence of mechanochemical effects, via processes involving solid-state configurational changes and structural rearrangements.^{1,3–5,7} Thermochemical mechanisms including liquid-phase reactions, founded on the observation of localized melts (or “hot spots”) at interparticle regions have also been proposed.^{8–13}

The highly exothermic nature of Mo-Si powder mixtures ($\Delta H_R = -31.5$ kcal/mol for MoSi₂; -74.5 kcal/mol for Mo₅Si₃) and the large differential in flow strength, density, and melt temperature between Mo and Si ($\Delta\sigma_y \sim 230$ MPa, $\Delta\rho = 7.9$ g/cm³, and $\Delta T_m = 800$ °C) make this an ideal system for investigating the effects of shock compression. In such highly exothermic powder mixtures, “shock-assisted” chemical reactions can also occur in shock-compressed powder compacts because of bulk shock temperature increases in the time scales of temperature equilibrium.¹⁴ Consequently, the observation of reaction products in recovered compacts,

during post mortem microstructural analysis (similar to those observed by Meyers *et al.*,^{8,13} Marquis and Batsanov,⁹ Montilla,¹² and Aizawa¹⁵), cannot provide information on whether the observed reaction may have occurred due to “shock-assisted” or “shock-induced” conditions.⁵ The inference of “shock-induced” chemical reactions requires *in situ* measurements of shock properties using time-resolved experiments. Post mortem microstructural analysis of recovered samples can, however, be used to characterize changes in the configuration of reactant constituents at conditions just prior to the onset of reaction initiation, to obtain clues for possible reaction mechanisms.¹⁴

Batsanov and his co-workers¹⁶ pioneered the use of time-resolved observations of chemically reacting powder mixtures using Manganin pressure gauges to obtain records of shock profiles and wave speed. They observed that in equimolar tin and sulfur powder mixtures the measured pressure points deviated toward the right (increased volume) of the Hugoniot curve calculated for the unreacted mixture. Additional work was reported in this same system¹⁷ and in the tin-telluride system,¹⁸ in which optical pyrometric measurements were also utilized. The aluminum-sulfur system was also investigated in work reported in 1992.¹⁹ Since that time, various other detection methods (including Manganin and polyvinyl difluoride (PVDF) stress gauges and optical and pyrometry measurements) have been employed for time-resolved diagnostics of shock-wave profiles.^{20–26} These studies (reviewed in Ref. 27) have provided a demonstration of the unique shock-compression response of powders, as well as the evidence for shock chemistry occurring on times

^{a)}Corresponding author: electronic mail: naresh.thadhani@mse.gatech.edu

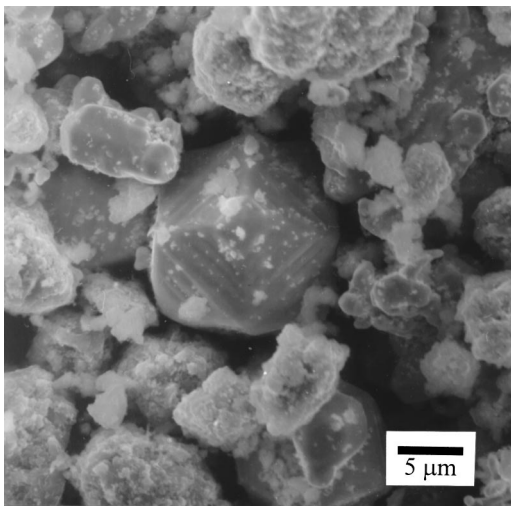


FIG. 1. Scanning electron micrograph of the Mo+2Si starting powder mixture.

scales of significantly less than the typical wave transit time of 1 μ s. Evidence of shock-induced chemical reactions has been inferred on the basis of shifts in the pressure-volume Hugoniot-curve, temperature changes, increases in shock-wave speed or bulk sound speed, and excess reflected-shock pressure monitored with time-resolved diagnostics.²⁷

In the present work, the shock-compression response of the highly exothermic Mo+2Si powder mixture, which includes constituents having a large differential in their physical and mechanical properties, was studied. The goal of this study was to employ time-resolved diagnostics of shock-wave profiles to detect the occurrence (or not) of “shock-induced” chemical reactions and the role of melting of the constituent(s) on initiation of such reactions. The overall approach involved shock compression experiments performed on ~58% dense Mo+2Si powder mixtures, using PVDF piezoelectric stress gauges, to measure the crush strength, compressibility characteristics, and wave propagation speed through the powder mixture. The analysis of the results and the conclusions presented in this paper retract the results described in our prior conference-proceedings publications.^{28–30}

II. EXPERIMENTAL PROCEDURE

Molybdenum and silicon powders were obtained from Cerac, Inc., with the particle size of $<44 \mu\text{m}$ (–325 mesh) and typical purity of 99.999% (Mo, M2000, and Si, S1049). The powders were mixed in a stoichiometric ratio corresponding to MoSi₂ intermetallic compound, using a slow moving V blender operated for 8–12 h. A scanning electron micrograph showing the typical morphology of the Mo and Si starting powder mixture is depicted in Fig. 1. The Mo powders were polycrystalline agglomerates, while Si powders were blocky single crystal particles.

Time-resolved measurements were performed using the Bauer piezoelectric polyvinyl difluoride stress gauges.^{31–34} The 80 mm diameter, 10 m long single stage, compressed-gas gun at Georgia Tech was used for the instrumented experiments. The gas gun provides control of “tilt” (typically

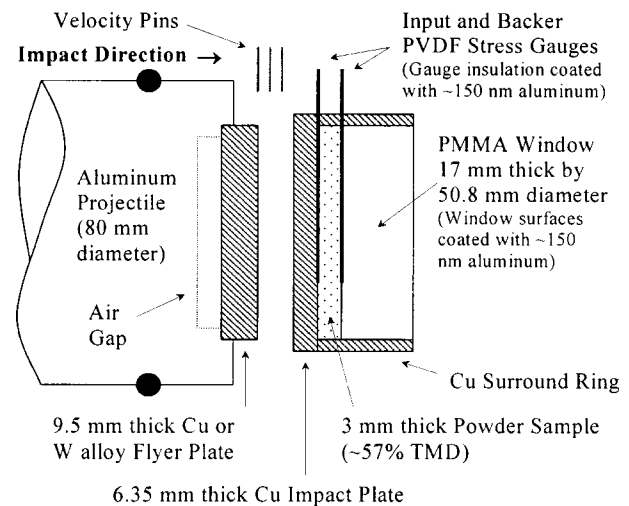


FIG. 2. Setup used for instrumented experiments with PVDF gauges sandwiching the 3 mm thick powder sample.

250 μ rad), impact velocity, and wave speed measurements to 0.1% accuracy. The frequency response of the PVDF stress gauges and recording system results in precise timing measurements available with the use of gigahertz frequency response instrumentation.

The gauges, obtained from KTech Corporation, in Albuquerque, N.M., were high quality, biaxially stretched PVDF film, poled using the Bauer process³¹ to a $9.2 \mu\text{C}/\text{cm}^2$ remnant polarization, and having identical gold over Pt electrodes. A typical PVDF gauge package configuration consists of an insulating film of FEP Teflon (25 μm thick) on both sides of a 25 μm thick PVDF element. During gauge assembly, typical total epoxy bond thickness was on the order of 2–4 μm . Aluminum deposition of ~200 nm on the powder sides of the gauge package was utilized to prevent pyroelectric effects from affecting the gauge response during densification and possible reaction of the powder mixture. The overall experimental arrangement employed for PVDF gauge measurements was similar to that at Sandia National Laboratories, in Albuquerque,^{33,34} and also used in the previous work on Ti-Si powder mixtures.²⁷ As shown in Fig. 2, a hollow aluminum projectile was used with either a copper or tungsten flyer plate (9.5 mm thick by 50.8 mm diameter) placed at the nose, backed by an air gap. The powder mixtures were pressed directly into copper capsules, consisting of a 20 mm thick Cu ring, in which the powder is sandwiched between a 6.35 mm thick Cu driver plate (toward the impact side) and a 17 mm thick polymethyl methacrylate (PMMA) backer plate. A PVDF gauge package (with 25 μm FEP polymer insulation epoxied on both sides) was placed between the packed powder and Cu driver plate to monitor the “input shock,” and between the powder and PMMA backer to monitor the “propagated-wave” loading characteristics. The propagation of the shock wave sensed by the “input” gauge and “propagated” gauge at their respective locations also provided a precise measure of the transit time through the powder mixture compact for determining the wave speed.

The sample assembly was placed on the impact surface of the gun barrel in which the smooth-bored projectile faced

with a 9.5 mm thick copper or tungsten alloy (MIL-T-21014) flyer plate was accelerated to a preselected impact velocity (in the range of 507 to 976 m/s). The impact velocities were measured using three shorting pins placed 12.7 mm apart and standoff pins placed 6.35 mm from the impact surface. It should be noted that all impact experiments were designed such that a planar-parallel shock wave propagates through the powder thickness without attenuation from loading or peripheral surfaces.

To improve sensitivity, the piezoelectric current was recorded with two complimentary amplifier sensitivities connected to a current viewing resistor at the PVDF gauge. The combined recordings of both amplifiers provide a high-resolution current-versus-time profile, which is then numerically integrated to obtain the stress-versus-time profile (using VIEWPOINT 3.16 software). The magnitude of the input stress was determined using data analysis procedures described elsewhere.^{33,34}

III. RESULTS OF TIME-RESOLVED EXPERIMENTS

Time-resolved experiments were performed on Mo + 2Si powder mixtures, using PVDF stress gauges placed between the Cu driver and powder (labeled “input gauge”), and the powder and PMMA backer plates (labeled “propagated” gauge). The loading configuration employed was such that the impact generates a shock-wave pulse of abrupt rise time, duration of constant pressure, and release to zero stress. Thicknesses of the driver and flyer plates were also such that the steady-state square shaped shock wave was transmitted through the thickness of the powder layer, without attenuation. All impact plane surfaces were lapped to ensure planarity such that the rise times recorded by the “input” gauges placed between the copper driver and Mo + 2Si powder were less than 10 ns. However, propagation of the stress wave through the powder mixture results in powder densification, which causes the wave to become more dispersed. The effect of the powder densification on wave dispersion is reflected by the increased rise time of the propagated stress wave recorded by the backer gauge placed at the interface between the powder and PMMA backer. It should be noted that during the steady-state stress period (duration of approximately a few microseconds in the present case), the gauge is highly stressed, but the rate of stress change is zero. The subsequent release of the stress to zero occurs later in time and is not observed in the recording window of the digital oscilloscopes. Thus the measured profiles show only the loading events, including the steady-state stress amplitude, but no unloading history.

A combined plot of the input stress traces for all experiments performed on Mo + 2Si powder mixtures is provided in Fig. 3. The propagated stress traces for all three low-velocity experiments are provided in Fig. 4(a) and the traces from the higher-velocity experiments are shown in Fig. 4(b). The varying amplitudes of the different stress profiles correspond to experiments performed at different impact velocities. As mentioned earlier, it can be clearly seen that the rise time of the input stress pulse is less than 10 ns under all impact conditions. In contrast, the propagated stress wave

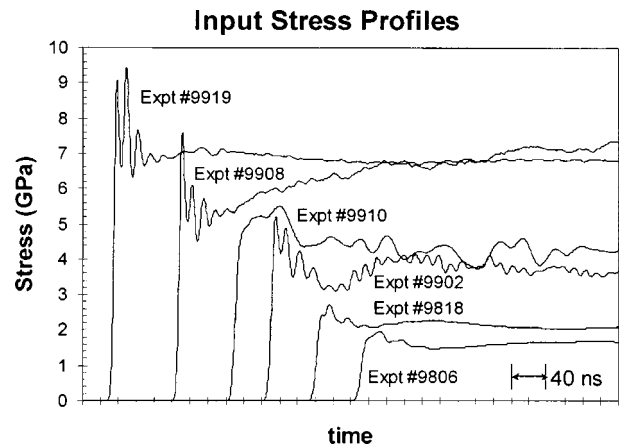


FIG. 3. Combined plot of the input stress traces for all experiments.

shows effects of wave dispersion and rise time varying between 6 and 186 ns, with the lower-amplitude stress waves showing the longest rise time.

A. Parameters measured from stress-gauge experiments

The parameters obtained from time-resolved stress-gauge measurements performed using shock-compression experiments on Mo + 2Si powder mixtures, are included in

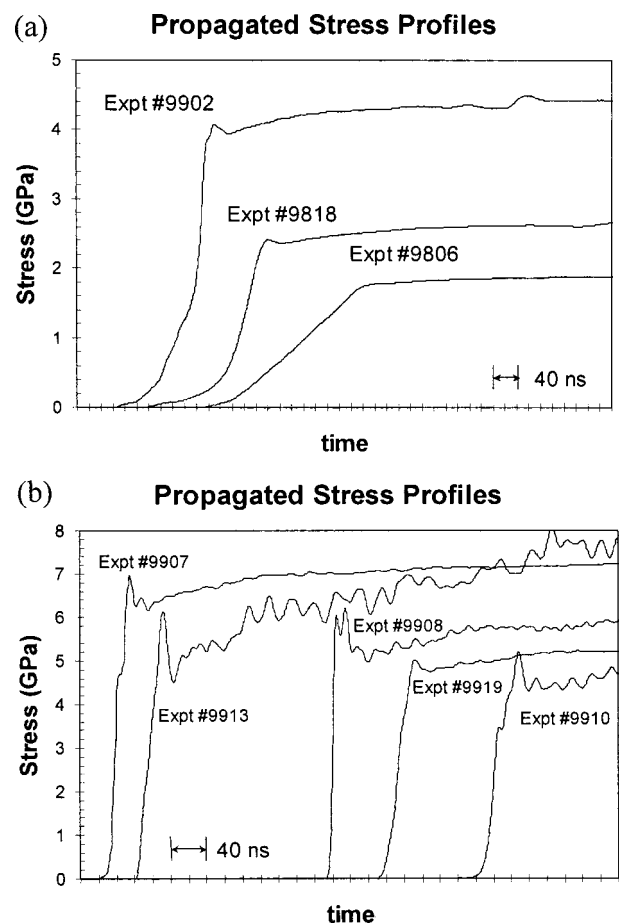


FIG. 4. Combined plot of the propagated stress traces for (a) all three low-velocity experiments and (b) the higher-velocity experiments.

TABLE I. Summary of results listing measured and calculated parameters obtained from time-resolved experiments.

Experiment no.	Flyer type	Packing density (g/cm ³ , %TMD)	Impact velocity (mm/μs)	Input stress (GPa)	Input rise time (ns) (10%–90%)	Propagated stress (GPa)	Propagated rise time (ns) (10%–90%)	Wave speed (mm/μs) (toe-toe 10%, 1/2 max)	Relative volume (toe-toe 10%, 1/2 max)
9806	Cu	2.59, 57	0.507	1.52	11.5	1.82	186	1.31, 1.26	1.17, 1.12
9818	Cu	2.50, 55	0.700	2.09	7.5	2.36	86	1.46, 1.44	1.12, 1.09
9902	Cu	2.69, 59	0.964	3.15	6.5	3.95	76.5	1.69, 1.64	1.01, 0.97
9910	W alloy	2.70, 59	0.851	4.36	8.5	4.30	10, 14 ^a	1.92, 1.91	0.97, 0.96
9908	W alloy	2.71, 59	0.940	5.4	4.5	5.18	6	2.15, 2.15	0.96, 0.96
9907	W alloy	2.71, 59	0.966	6.3 ^b	^c	6.16	8.7 ^a	2.04 ^b	0.75 ^b
9913	W alloy	2.50, 55	0.967	6.3 ^b	^c	5.07	22.5	2.12 ^d	0.81
9919	W alloy	2.51, 55	0.914	6.65	5	4.74	25.5	2.22, 2.20	0.84, 0.83

^aTwo-slope wave structure.^bCalculated value.^cNo measurement obtained.^dToe-to-toe measurement at shock arrival instead of 10%.

Table I. As indicated in the table, the shock-loading experiments were performed at impact velocities in the range of 0.507 to 0.964 mm/μs using a copper flyer plate, and 0.851 to 0.967 mm/μs using a tungsten alloy flyer plate. Experiments with the tungsten flyer were used to obtain higher input stresses. In all cases, the initial powder packing density was maintained approximately the same $\sim 58\% \pm 2\%$ theoretical maximum density (TMD).

In Table I, data in the input stress column correspond to the stress in the powder measured by the input-shock gauge, by the method described above. The rise time of the input stress wave is measured based on 10–90% of the peak and shows that in all cases the rise to peak stress occurs in less than 10 ns. Data in the propagated stress column correspond to the stress measured in the PMMA backer upon exiting the powder layer. The propagated stress rise time is longer for experiments performed at lower impact velocities, but decreases significantly in experiments at higher impact velocities. The wave speed is the wave velocity through the powder, and is obtained by measuring transit time between the two gauges placed in direct contact with opposite surfaces of the powder, less the travel time through the gauge insulation thickness. The transit time was measured based on toe-to-toe (10%) and transit times between half-maximum values with the insulation thickness subtracted. The time was then used to calculate the powder wave speed using the following equation:

$$U_s = x_{\text{powder}} / t_{\text{transit}} \quad (1)$$

In this equation, U_s is the powder shock speed, x is the powder thickness, and t_{transit} is the measured transit time between the two gauges.

The relative volume V/V_0 , the only calculated parameter shown in Table I, was obtained from the known initial

powder (ρ_{00}) and solid density (ρ_0), measured values of input stress (P), and wave velocity (U_s), and applying the shock jump conditions for conservation of mass and momentum:

$$(V/V_0) = (\rho_0/\rho_{00}) \{1 - (P/\rho_{00}U_s)(1/U_s)\} \quad (2)$$

Since the stress pulses propagating through the 3 mm thick powder mixtures have a structure characteristic of wave-dispersion effects [as observed in Figs. 4(a) and 4(b)], calculation of the relative volume based on Eq. (2) using jump conditions applied to a steady-state shock wave may not be completely appropriate. However, given the very large compression achieved with such porous materials, one can use the calculated relative volume along with measured input stress to obtain first-order effects of shock compression of Mo+2Si powder mixtures.

B. Correlation of stress versus volume and stress versus wave speed

The plot of data points corresponding to the measured input stress as a function of calculated relative volume and that for measured input stress versus wave speed for the Mo+2Si powder mixture are shown in Figs. 5 and 6, respectively. It should be noted that the plot in Fig. 5 is different from that reported in our prior publications,^{28–30} in which the relative volume was erroneously calculated. Therefore, the analysis provided here in the following section retracts the discussions and conclusions previously stated in that work. Figure 5 shows two sets of data points for each pressure, corresponding to relative volumes calculated using the two values of the wave speeds based on toe-to-toe and half-max measurements. The data point corresponding to the initial relative volume of the powder and the calculated compress-

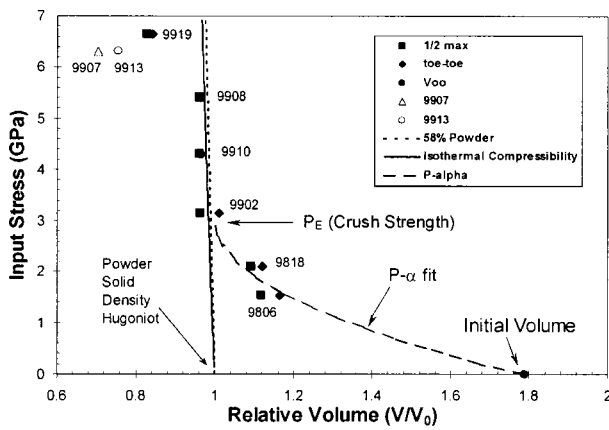


FIG. 5. Plot of measured input stress versus calculated relative volume for Mo+2Si powder mixture based on instrumented experiments with the $P-\alpha$ curve fit to the lower-pressure data points and isothermal compressibility curve.

ibility curves (Hugoniot) of solid-density Mo+2Si (dashed line) and MoSi₂ solid (solid line) are also indicated on the plot. Data corresponding to the measured input stress versus wave speed plotted in Fig. 6 are also based on wave speed calculated using toe-to-toe and half-max values.

Special considerations were made in plotting the data points for experiments 9907 and 9913, in both the stress versus volume and stress versus wave speed plots. In the case of experiment 9907, an input gauge record was not obtained (due to gauge failure), and for experiment 9913, a gauge signal and impact velocity were recorded, but the gauge output signal did not allow a stress measurement and provided only shock-wave time of arrival information. The impact velocity was, however, correctly measured in both experiments. Therefore, the input stress at the copper-powder interface was calculated for both experiments using two steps. First, the stress in the copper plate was calculated using the known impact velocity and the Hugoniot relationships for the tungsten flyer and copper driver plates. Next, this pressure was utilized along with the Hugoniot of copper

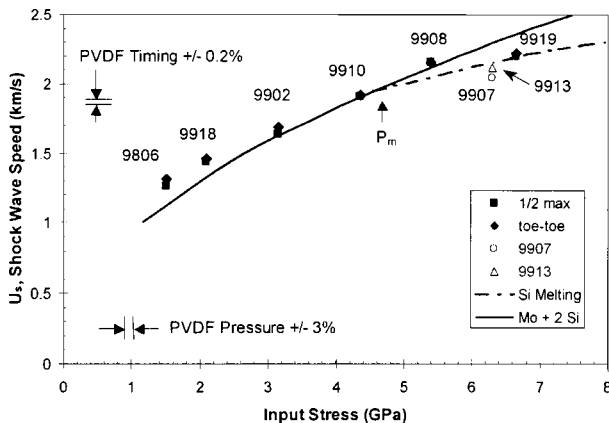


FIG. 6. Plot of input stress as a function of powder wave speed. Data for Experiment 9907 based on calculated values of wave speed and input stress and those for Experiment 9913 based on calculated value of input stress and measured wave speed. Note mixture curve and silicon behavior (P_m indicates melting point of silicon for ~58% dense powder mixture).

and a calculated Hugoniot relationship (approximated using the lower-velocity instrumented experiments) for the Mo +2Si powder mixture to determine the input stress at the copper-powder interface. For experiment 9913, the calculation of the relative volume was performed using the measured wave speeds, calculated pressure at the copper-powder interface, and the equations for the conservation of mass and momentum. Because no input gauge signal was measured for experiment 9907, the time of arrival of the shock wave was also calculated. Since the impact velocity was known along with the trigger pin standoff height (nominally 6.35 mm), the time of impact at the tungsten flyer and copper driver interface could be easily calculated. Utilizing the pressure in the copper plate and the measured plate thickness, the travel time through the copper plate was then calculated which yielded a calculated shock wave arrival time at the copper-powder interface. The remaining calculation of relative volume for experiment 9907 was performed with the calculated values for both the input stress and the shock-wave arrival time.

It should be noted that in both plots, Figs. 5 and 6, two sets of data points are indicated for each pressure, corresponding to wave speeds measured on the basis of toe-to-toe and half-max values of stress profiles. Of the two measurements of the wave speed, the measurement based on half-max values can be considered to be more representative due to the slow rise in the toe of the dispersed propagated wave. In particular, low-amplitude propagated wave stress profiles [as shown in Figs. 4(a) and 4(b)] have a very shallow toe that can add to the additional discrepancy in determination of the wave speed. The significance of the results based on input stress versus relative volume (Fig. 5) and input stress versus wave speed (Fig. 6) will be discussed in detail in the following section.

IV. ANALYSIS OF SHOCK-COMPRESSION CHARACTERISTICS BASED ON TIME-RESOLVED EXPERIMENTS

In the present work, time-resolved experiments employing PVDF stress gauges were performed on Mo+2Si powder mixtures, to record the “input” stress-wave profiles and the “propagated” stress-wave profiles, as illustrated in the experimental setup shown in Fig. 2. The recorded input stress-wave profiles are shown in Fig. 3 and the propagated stress wave forms are shown in Figs. 4(a) and 4(b). Other than the effects of wave reverberation through the PVDF gauge package, which appear to resemble vibration signals as the pressure equilibrates, no obvious signature is revealed by the “input” stress gauge profiles. The propagated stress profiles, however, reveal a longer rise time, particularly in the stress profiles of lower magnitude [Fig. 4(a)]. The increase in rise time is due to dissipative processes responsible for powder densification, which causes the wave to become more dispersed. The effect of powder densification on wave dispersion is most clearly observed in propagated wave profiles for which the input stress is less than the “crush strength” of the powder mixture, or the stress required to consolidate the Mo+2Si powder mixtures to full density. Consequently, the higher-amplitude “propagated” stress-

wave profiles shown in Fig. 4(b) (corresponding to experiments 9910, 9908, and 9919) reveal minimal effects of wave dispersion.

Experimental measurements of the “input” and “propagated” stress-wave profiles also provides a measure of the wave speed, by noting the time of travel of the wave through a given thickness of the powder layer. Since, in shock compression, the input stress (or shock pressure) entering the powder and the speed of the wave (shock velocity) propagating through the powder layer are inter-dependent, a sudden change in their interdependence could be conceived as a signature of a “shock-induced” physical or chemical change. Furthermore, assuming steady-state propagation of a shock wave through the powder mixture, jump conditions correlating the state variables ahead of and behind the shock front can be used to determine pressure versus specific volume (compressibility) behavior to identify discontinuities corresponding to physical or chemical changes. Evidence of shock-induced chemical reactions based on observation of expanded pressure-volume state and increased shock wave velocity has been demonstrated in previous investigations.^{16–19,27}

A. Pressure-volume compressibility behavior

The measured input stress plotted as a function of calculated relative volume for the Mo+2Si powder mixture in Fig. 5 shows the general Hugoniot (compressibility) behavior of the un-reacted powder mixture and solid MoSi₂, illustrating the manner in which the powder mixture compresses to the solid-density state. The stress at which the powder mixture constituents compress to solid density is defined as the “crush strength.” It is during this process of powder crush up to full density that a configuration of extensively deformed, intimately mixed, and highly activated state of reactants is generated. Consequently, at pressures approaching the crush strength, reactive powder mixtures can undergo “shock-induced” chemical reactions. The compressibility response of Mo+2Si powder mixtures studied in the present work, illustrates that the data points are clustered in three different regions (as shown in Fig. 5); hence, a single curve cannot be used to fit the data and describe the overall compressibility behavior of this powder mixture. Each cluster of data points thus needs to be discussed separately.

Densification of the powder mixture from an initial to final solid density was considered first, using the P - α pore collapse model.³⁵ The P - α model uses a distension parameter α defined by $\alpha = V/V_s$, where V is the specific volume of porous material and V_s is the specific volume of the solid.

Accordingly, the P - α model is expressed by the equation

$$\alpha = 1 + (\alpha_p - 1) [(P_s - P)/(P_s - P_E)]^2. \quad (3)$$

In this equation, α_p is the density achieved during elastic compression, P_E is the pressure where elastic compression is observed, and P_s is the crush strength. Because the P - α model is rather empirical, the parameters α_p , P_E , and P_s were adjusted to best fit the experimentally obtained data. Figure 5 displays the P - α model results superimposed to fit

the three low-pressure data points on the P - V curve for Mo+2Si. The value of P_E was found to be 0.05 GPa, α_p was 1.75, and P_s (full densification) was determined to be 3.0 GPa for the best fit of the P - α densification curve to the data points. The second cluster of data points (starting at 3.1 GPa, for experiments 9902, 9910, and 9908) in Fig. 5 follows the Hugoniot line of the solid-density mixture, representing full densification of the powder. However, in the case of the 3.1 GPa data point, the toe-to-toe and half-max values do not fully coincide, while the points at 4.3 and 5.4 GPa are equal in both cases. Because the toe-to-toe values will be slightly different from half-max values if wave-dispersion effects dominate the shock-compression response, the true crush strength can be considered to be slightly greater than 3.1 GPa. It should be noted that the experimental points in this region lie slightly to the left of both the calculated isothermal and 58% dense powder compressibility curves. It is uncertain if this discrepancy is due to slight systematic experimental errors (error bars slightly larger than plotting symbols), incorrect assumptions to some extent in the calculation of the mixture rule based compressibility curves, or both. In any case, these errors appear to be small. The final cluster of points (for experiments 9907, 9913, and 9919) above 6 GPa in Fig. 5 indicates an even more compressed state than that of the solid-density curve. The deviation from the solid density to a more compressed state is a clear indication of a “shock-induced” change that needs to be further explored.

B. Shock-wave speed versus input stress

While the input stress (pressure) versus volume compressibility behavior is based on the use of jump conditions, which may be argued to represent first-order effects of shock compression, the correlation between measured shock-wave speed versus measured input stress provides a behavior that is independent of assumptions. The calculated curve corresponding to the 58% dense inert Mo+2Si powder mixture is also illustrated as a dashed line in Fig. 6. It can be seen that the experimental data points appear to follow the inert Hugoniot curve, except at stresses greater than 6 GPa.

Prior work on time-resolved measurements in Ti-Si powder mixtures²⁷ has shown deviation of the experimentally determined data points from the calculated Ti-Si inert powder mixture curve at input stresses exceeding the 1.5 GPa crush strength of the material. The deviation indicating an increase in wave speed and likewise an expanded pressure-volume compressibility state was considered to be an overt indication of “shock-induced” chemical reaction. An expanded pressure-volume compressibility state (first observed by Batsanov *et al.*¹⁶ in Sn+S powder mixtures) with corresponding increase in shock wave speed, is consistent with the occurrence of “shock-induced” (also termed “ballotechnic”) chemical reactions proposed by Graham *et al.*²⁴ and modeled by Bennett and Horie.³⁶ However, in the case of the present work on Mo+2Si powder mixtures, the deviation in the wave speed versus input stress curve actually shows a decreasing trend at stresses greater than 6 GPa. The decrease in wave speed is possible only if there is a “shock-induced” change to a low-compressibility state such as from the solid

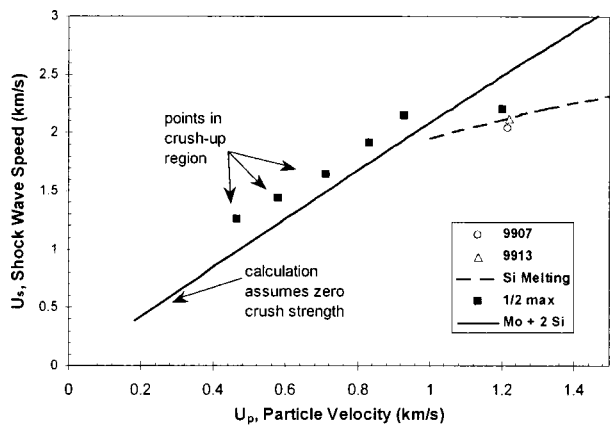


FIG. 7. Plot of shock wave speed (U_s) as a function of particle velocity (U_p) for measured data points, Mo+2Si ($\sim 58\%$ dense) calculated line, and silicon behavior.

to a liquid phase of possibly the silicon powder constituent.

Using the experimentally determined $U_s - U_p$ Hugoniot of melted silicon, obtained from Ref. 23, a curve corresponding to wave speed versus stress was calculated and plotted with the results of the present work, as shown in Fig. 6. It can be seen that the curve for melted silicon (dash-dotted line) intersects the Mo+2Si inert curve at P_m (~ 5 GPa) which represents the stress at which Si in the $\sim 58\%$ dense Mo+2Si powder mixture undergoes melting. The data points corresponding to the higher-pressure experiments are found to lie more closely on the silicon melt curve than on the curve of the Mo+2Si solid-density powder mixture. The cluster of these data points is also the same as the group of data points on the input stress versus relative volume (compressibility) plot shown in Fig. 5 that were observed to deviate from the solid-density curve to a more compressed state. Hence, it can be concluded that the deviation of the data points at stresses greater than 6 GPa, showing a higher-compressibility state and correspondingly lower shock speed (consistent with the slope of the Rayleigh line) indicate melting of silicon and not necessarily evidence of a “shock-induced” chemical reaction.

C. Shock-wave speed versus particle velocity

The wave speed versus input stress data points in Mo+2Si were converted to wave speed versus particle velocity (where particle velocity $U_p = P/\rho_0 U_s$). Since the shock wave speed is linearly related to the particle velocity, a deviation from linearity can be considered to be unambiguous evidence of chemical or physical change of state in the material. Figure 7 shows a $U_s - U_p$ plot of Mo+2Si powder mixture, along with calculated curves for the inert reactant powder mixture, as well as that of the silicon melt. It can be seen that the three experimental data points at lower particle velocities show higher shock-wave speeds than that calculated for the inert Mo+2Si mix. This is because the calculated curve is based on the assumed crush strength being zero. The next two data points between $U_p = 0.8$ and 1.0 closely approach the calculated curve of Mo+2Si. With further increase in particle velocity, the data points show a de-

crease in shock-wave speed and in fact fall on the $U_s - U_p$ curve of the silicon melt. The deviation from linearity in this case can again be associated with the melting of the silicon reactant.

Melting of silicon has also been observed in time-resolved experiments performed on 55% dense Nb+2Si powder mixtures in which the arrival of shock and rarefaction waves was recorded using a streak camera.²³ In fact, in experiments performed under identical shock compression conditions at shock pressures in the range of 5–20 GPa, it was observed that in some cases the measured shock data showed a trend indicating melting of silicon and in some other cases formation of NbSi₂ product. Melting of silicon and the corresponding lack of reaction product formation was attributed to the detrimental effect of premature melting of silicon and its limited mixing with niobium, thereby inhibiting the initiation of “shock-induced” chemical reaction. For the present work on $\sim 58\%$ dense Mo+2Si powder mixtures, only melting of Si was observed with no evidence of shock-induced chemical reaction occurring in the range of 6–7 GPa shock pressure.

The results of the present work on Mo-Si powder mixtures, taken in conjunction with Nb-Si and Ti-Si powder mixtures, illustrate clear differences in the shock-compression response of these three silicide-forming systems, with the melting of silicon possibly influencing the overall shock-compression response of the respective systems. This leads to an important question which will be discussed in the following section: What is the influence of melting of silicon (during shock compression) on the shock-compression response and reaction behavior of powder mixtures?

D. Influence of silicon melt on shock-induced reaction initiation

The results of time-resolved measurements performed on the three different silicide-forming systems indicate that melting of Si appears to inhibit shock-induced chemical reaction initiation as observed in both Nb-Si and Mo-Si powder mixtures, while Ti-Si powder mixtures show occurrence of shock-induced reaction evidenced by observation of expanded pressure-volume state and increased shock speed associated with the reaction. These results are consistent with the observations of a theoretical study conducted by Tamura and Horie.³⁷ They investigated reaction initiation in Nb+Si powder mixtures inside regions of an adiabatic shear band and observed that increasing shear rate resulted in greater degree of thinning (deformation) of reactants and consequently both mixing and increased propensity for shear-induced solid-state reaction. However, with increased shearing rate, if temperature of silicon was allowed to increase [due to its lower value of the product of density and heat capacity (ρC_p)] above its melt temperature, then the degree of mixing between solid niobium and liquid silicon was reduced, which in turn inhibited reaction initiation. In fact, they established a critical shear rate, above which melting of silicon was always observed, leading to a loss of its shear and tensile strength, and subsequently resulting in its behaving more like a fluid and inhibiting reaction initiation. Hence,

it appears that “shock-induced” chemical reactions in powder mixtures can occur during the process of crush-up to solid density, similar to the trends observed in Ti-Si.²⁷ However, premature melting of a constituent and its capillary flow around the particles of the other constituent (e.g., Mo, Nb) will result in insufficient deformation and plastic flow of the latter, due to its being subjected to hydrostatic rather than deviatoric compression. Consequently, mixing between the reactants will be limited, resulting in inhibition of the initiation of “shock-induced” chemical reactions.

The premature melting of silicon during the powder crush-up process, and its consequent effect on “shock-induced” chemical reaction initiation, is related to the mechanism(s) responsible for such reactions. If thermal initiation of reactions based on melting of silicon is considered as a mechanism for “shock-induced” chemical reaction, then the reaction threshold for all Si-based powder mixture systems ought to be identical. Consequently, the shock pressure that results in melting of silicon (~ 5 GPa for 55% density) would be considered as the threshold shock pressure for reaction initiation. However, shock-induced chemical reactions have been observed to occur in $\sim 55\%$ dense Ti-Si powders²⁷ at ~ 1.5 GPa shock pressure, which is significantly lower than the ~ 5 GPa pressure required for melting of silicon. Likewise, no evidence of shock-induced chemical reaction is observed in Mo-Si powders even at shock stresses in the 6–7 GPa range.

The pressure threshold for “shock-induced” chemical reactions can be correlated with the crush strength of the powder mixtures, which in turn scales with the differential in the yield strengths of the constituents of the powder mixture. The yield strength differential between reactants in Mo-Si ($\Delta\sigma_Y^{\text{Mo-Si}} = 400-93$ MPa) and Nb-Si ($\Delta\sigma_Y^{\text{Nb-Si}} = 207-93$) is greater than that in Ti-Si ($\Delta\sigma_Y^{\text{Ti-Si}} = 59-93$ MPa); consequently the crush strength of Mo-Si and Nb-Si powder mixtures is greater than that of Ti-Si. Consideration of the influence of melting of silicon during crush-up indicates that, if the crush strength of the powder mixture is greater than the melt pressure of Si, then premature melting of silicon can be expected. Consequently, the silicon melt will restrict mixing between reactants, which can inhibit the initiation of “shock-induced” chemical reaction. If, on the other hand, the crush strength of the powder mixture is lower than the melt pressure of silicon, then mixing of the reactants due to plastic deformation and dispersion can be achieved during the crush-up process, which can lead to initiation of “shock-induced” chemical reactions.

V. SUMMARY AND CONCLUSIONS

Time-resolved experiments performed on $\sim 58\%$ dense Mo+2Si powder mixtures employing in-situ PVDF stress gauges were used to record the input wave and propagated wave stress profiles, as well as the speed of the wave propagation through the thickness of the powder, for impact experiments at velocities in the range of 0.5 to 1 km/s (with Cu and W alloy flyer plates). Input stress profiles of ~ 1.5 to 6.7 GPa amplitude and rise times of 4.5–11.5 ns were recorded, while the corresponding propagated stress profiles were of

~ 1.8 to 6.2 GPa magnitude and rise times of ~ 6 to ~ 190 ns. The velocity of the shock wave propagating through the $\sim 58\%$ dense Mo+2Si powder mixtures under the above impact conditions were in the range of 1.3–2.2 km/s. Analysis of the time-resolved experiments performed on $\sim 58\%$ dense Mo+2Si powder mixtures at input stresses less than 4 GPa show characteristics of densification, based on the data points falling on the curve corresponding to powder crush-up represented by the P - α densification behavior, and dispersed nature of propagated wave stress profiles with rise time greater than ~ 40 ns. In the time-resolved experiments performed at input stress between 4 and 6 GPa, the powder mixtures showed characteristics of following the fully densified mixture. For stresses between 6 and 7 GPa, the data points indicate melting of silicon denoted by a decrease in volume and wave speed, and no evidence of shock-induced chemical reactions in the range of the experiments performed in this study. Results of the present work on Mo-Si, taken in conjunction with prior work on Nb-Si and Ti-Si systems, illustrate that premature melting of silicon and its capillary flow can limit the deformation and mixing between reactants, thereby inhibiting the initiation of “shock-induced” chemical reactions.

ACKNOWLEDGMENTS

This research was funded by the Army Research Office under Grant Nos. DAAH0495-1-0235 and DAAG55-97-1-0163. The partial stipend support provided by the Georgia Institute of Technology Molecular Design Institute, under Prime Contract N00014-95-1-1116 from ONR, is also acknowledged.

- ¹A.N. Dremin and O.N. Bruesov, *Russ. Chem. Rev.* **37**, 392 (1968).
- ²G. Duvall, National Materials Advisory Board Report No. 414, National Academy Press, Washington D.C., 1984.
- ³R.A. Graham, B. Morosin, E.L. Venturini, and M.J. Carr, *Annu. Rev. Mater. Sci.* **16**, 315 (1986).
- ⁴N.N. Thadhani, *Prog. Mater. Sci.* **37**, 117 (1993).
- ⁵N.N. Thadhani, *J. Appl. Phys.* **76**, 2129 (1994).
- ⁶S.A. Sheffield, D.D. Bloomquist, and C.M. Tarver, *J. Chem. Phys.* **80**, 3831 (1984).
- ⁷R.A. Graham, in *Proceedings of the 3rd International Symposium on High Dynamic Pressures*, edited by R. Charet (Association Francaise de Pyrotechnie, Paris, 1989), pp. 175–180.
- ⁸M.A. Meyers, L.-H. Yu, and K.S. Vecchio, *Acta Metall. Mater.* **42**, 701 (1994); **42**, 715 (1994).
- ⁹F.D.S. Marquis and S.S. Batsanov, in *Powder Material: Current Research and Industrial Practices* (TMS, Warrendale, PA, 1999), pp. 113–128.
- ¹⁰B.R. Krueger, A.H. Muntz, and T. Vreeland, Jr., *Metall. Trans. A* **23**, 55 (1991).
- ¹¹T. Vreeland, Jr., *Scr. Metall.* **38**, 337 (1998).
- ¹²K. Montilla, Ph.D. thesis, California Institute of Technology, 1997.
- ¹³M.A. Meyers, S.S. Batsanov, S.M. Gavrilkin, H.C. Chen, J.C. LaSalvia, and F.D.S. Marquis, *Mater. Sci. Eng., A* **201**, 150 (1995).
- ¹⁴K.S. Vandersall and N.N. Thadhani, *Metall. Mater. Trans. A* **34**, 15 (2003).
- ¹⁵T. Aizawa and B.K. Yen, in *Shock Compression of Condensed Matter—1997*, edited by S.C. Schmidt, D.P. Dandekar, and J.W. Forbes, AIP Conf. Proc. No. 429 (AIP, Woodbury, NY, 1998), pp. 651–654.
- ¹⁶S.S. Batsanov, G.S. Doronin, S.V. Klochkov, and A.I. Teut, *Combust., Explos. Shock Waves* **22**, 134 (1986).
- ¹⁷S.S. Batsanov, M.F. Gogulya, M.A. Brazhnikov, G.V. Simakov, and I.I. Maksimov, *Combust., Explos. Shock Waves* **36**, 361 (1994).
- ¹⁸S.S. Batsanov, M.F. Gogulya, M.A. Brazhnikov, E.V. Lazareva, G.S.

- Doronin, S.V. Klochkov, M.B. Banskikova, A.V. Fedorov, and G.V. Simakov, *Sov. J. Chem. Phys.* **10**, 1699 (1991).
- ¹⁹M.F. Gogulya, I.M. Voskoboinikov, A. Yu Dolgoborov, N.S. Dorokhov, and M.A. Brazhnikov, *Sov. J. Chem. Phys.* **11**, 343 (1992).
- ²⁰M.B. Boslough, *Phys. Chem. Lett.* **160**, 618 (1989).
- ²¹M.B. Boslough, *J. Chem. Phys.* **92**, 1839 (1990).
- ²²X. Gao and F. Jing, in *Proceedings of Condensed Matter Under Shock Pressures, 1991, Bombay, India*.
- ²³M. Yoshida and N.N. Thadhani, in *Shock Waves in Condensed Matter—1991*, edited by S.C. Schmidt, R.D. Dick, J.W. Forbes, and D.G. Tasker (Elsevier, Lausanne, 1992), pp. 586–592.
- ²⁴R.A. Graham, M.U. Anderson, Y. Horie, S-K You, and G.T. Holman, *Shock Waves* **3**, 79 (1993).
- ²⁵K.R. Iyer, L.S. Bennett, F.Y. Sorrell, and Y. Horie, in *High-Pressure Science and Technology—1993*, edited by S.C. Schmidt, J.W. Shaner, G.A. Samara, and M. Ross, AIP Conf. Proc. No. 309 (AIP, New York, 1994), pp. 1337–1340.
- ²⁶X. Chen, X. Jin, and Y. Musang, *Chin. J. High Press. Phys.* **3**, 67 (1994).
- ²⁷N.N. Thadhani, R.A. Graham, T. Royal, E. Dunbar, M.U. Anderson, and G.T. Holman, *J. Appl. Phys.* **82**, 1113 (1997).
- ²⁸K.S. Vandersall and N.N. Thadhani, in *Shock Compression of Condensed Matter—1999*, edited by M.D. Furnish, L.C. Chhabildas, and R.S. Hixson, AIP Conf. Proc. No. 505 (AIP, Melville, NY, 2000), pp. 763–766.
- ²⁹K.S. Vandersall and N.N. Thadhani, in *Proceedings of EXPLOMET 2000, International Conference on Fundamental Issues and Application of Shock-Wave and High-Strain-Rate Phenomena, Albuquerque, N.M., 2000* (to be published).
- ³⁰K.S. Vandersall and N.N. Thadhani, in *Shock Compression of Condensed Matter—2001*, edited by M.D. Furnish, Y. Hone, and N.N. Thadhani, AIP Conf. Proc. No. 620 (AIP, Melville, NY, 2000), pp. 1109–1112.
- ³¹F. Bauer, US Patent No. 4,684,337 (4 August 1987).
- ³²W.H. Holt, W. Mock, Jr., M.U. Anderson, G.T. Holman, and R.A. Graham, in *Shock Compression of Condensed Matter—1995*, edited by S.C. Schmidt and W.C. Tao, AIP Conf. Proc. No. 370 (AIP, Woodbury, NY, 1996), pp. 573–576.
- ³³M.U. Anderson and R.A. Graham, in *Shock Compression of Condensed Matter—1995* (Ref. 32), pp. 1101–1104.
- ³⁴R.A. Graham, M.U. Anderson, F. Bauer, and R.E. Setchell, in *Shock Compression of Condensed Matter—1991* (Ref. 23), pp. 883–886.
- ³⁵M.M. Carroll and A.C. Holt, *J. Appl. Phys.* **43**, 1626 (1972).
- ³⁶L.S. Bennett and Y. Horie, *Shock Waves* **4**, 127 (1994).
- ³⁷S. Tamura and Y. Horie, *J. Appl. Phys.* **84**, 3574 (1998).